



OPEN ACCESS

EDITED BY

Xunhua Zhang,
Qingdao Institute of Marine Geology
(QIMG), China

REVIEWED BY

Jianhui Jin,
Fujian Normal University, China
Qi Su,
Beijing Normal University, China

*CORRESPONDENCE

Ruonan Tian,
✉ 20rntian@stu.edu.cn
Zhongping Lai,
✉ zhongping_lai@stu.edu.cn

SPECIALTY SECTION

This article was submitted to Marine
Geoscience,
a section of the journal
Frontiers in Earth Science

RECEIVED 04 November 2022

ACCEPTED 30 March 2023

PUBLISHED 11 April 2023

CITATION

Zhong J, Liu B, Ou Y, Tian R, Shan J, Xu Y,
Wang F, Abbas M, Zhang K and Lai Z
(2023), An erosive neritic area of Shantou
in coastal NE South China Sea since at
least MIS 5 revealed by OSL dating
of cores.

Front. Earth Sci. 11:1089946.

doi: 10.3389/feart.2023.1089946

COPYRIGHT

© 2023 Zhong, Liu, Ou, Tian, Shan, Xu,
Wang, Abbas, Zhang and Lai. This is an
open-access article distributed under the
terms of the [Creative Commons
Attribution License \(CC BY\)](https://creativecommons.org/licenses/by/4.0/). The use,
distribution or reproduction in other
forums is permitted, provided the original
author(s) and the copyright owner(s) are
credited and that the original publication
in this journal is cited, in accordance with
accepted academic practice. No use,
distribution or reproduction is permitted
which does not comply with these terms.

An erosive neritic area of Shantou in coastal NE South China Sea since at least MIS 5 revealed by OSL dating of cores

Jiemei Zhong¹, Bohui Liu¹, Yang Ou¹, Ruonan Tian^{1*},
Jingxiang Shan¹, Yantian Xu², Feng Wang¹, Mahmoud Abbas ¹,
Ke Zhang³ and Zhongping Lai^{1*}

¹Institute of Marine Sciences, Guangdong Provincial Key Laboratory of Marine Disaster Prediction and Prevention, Shantou University China, and Southern Marine Science and Engineering Guangdong Laboratory (Zhuhai), Zhuhai, China, ²School of Geography and Tourism, Jiaying University, Meizhou, China, ³Guangdong Provincial Key Laboratory of Geodynamics and Geohazard, School of Earth Science and Engineering, Sun Yat-sen University, Guangzhou, China

The neritic region of the Chaoshan plain is located on the northeastern (NE) boundary of the South China Sea (SCS). Despite the extensive research on the stratigraphic architecture and sedimentary processes within the Chaoshan plain, the neighboring neritic area remains largely unexplored. In this study, we provide a new set of ages on seventeen quartz optically stimulated luminescence (OSL) dating results from four cores (SY2-2, SY3-1, SY3-2, and HS02) to investigate the regional chronostratigraphy and sedimentology of the area. The samples were collected at depths ranging from 0.6 to 73.5 m and yielded ages ranging from 4.9 ± 0.3 ka to $>139 \pm 28$ ka. Sedimentation thickness from cores SY3-2, SY2-2, and HS02 is less than 4.2 m, 5.5 m, and 6.4 m, respectively, since at least Marine Isotope Stage (MIS) 5, and the Holocene sediments of core SY3-2 are less than 4.2 m thick. The preservation state of the sediments in the area is poor since at least 83.6 ka, indicating an intensified erosion in the neritic region of the northeastern South China Sea (NESCS) since at least MIS 5. This erosion may have been caused by fluvial incision resulting from sea-level decline during the last glacial period, as well as strong transportation caused by coastal currents.

KEYWORDS

OSL dating, drilling cores, Chaoshan plain, South China sea, sedimentary environment

1 Introduction

The continental shelf is a vital component in sedimentation and the land-sea interaction, holding significant geological information such as changes in sea level, tectonic activity, and sedimentary processes (Li et al., 2014; Wang et al., 2019; Qin et al., 2023; Wang et al., 2023). The eastern continental shelf of China is abundant in Quaternary sediments with thicknesses exceeding 10 m since the Holocene (Wang et al., 2020). For instance, the Holocene sediments thicknesses recorded from core samples in the Bohai Sea and the south Yellow Sea are around 15 and 13 m thick, respectively (Liu et al., 2010; Lan et al., 2018; Chen et al., 2020; Long et al., 2022). Studies on the inner shelf of the East China Sea have mainly yielded a paleoclimate record since the Last Deglaciation, with thickness of the Holocene sediments approximately 20 m

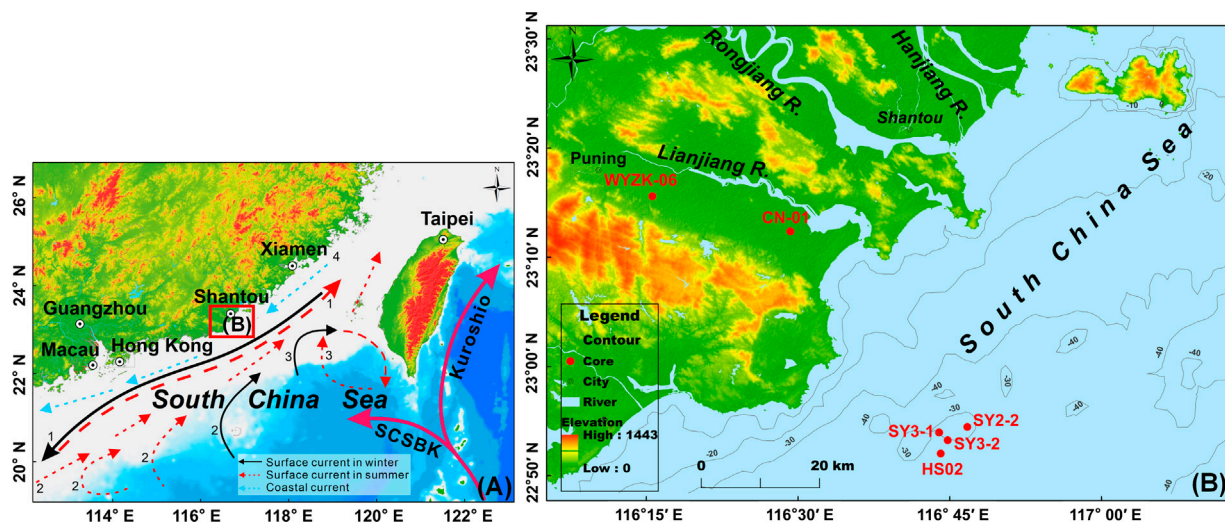


FIGURE 1

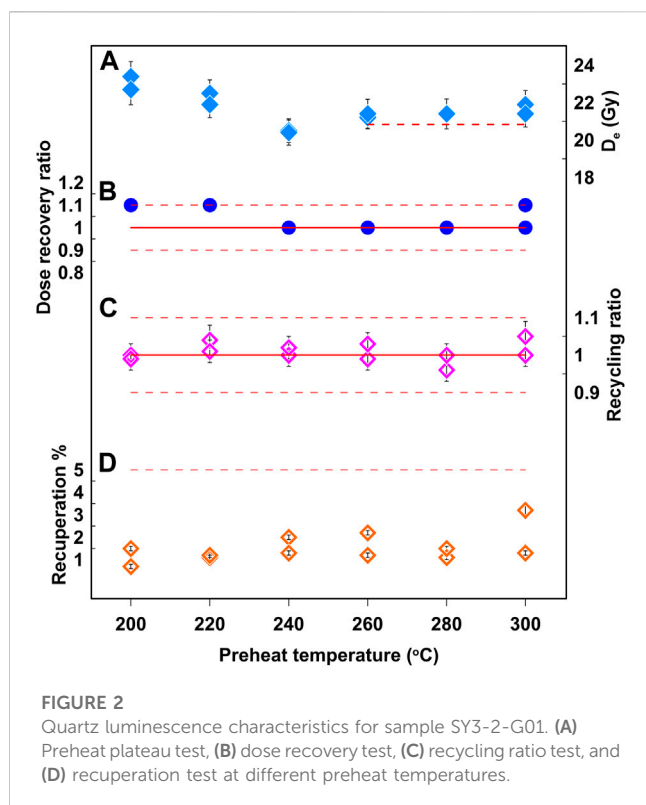
Location of the Chaoshan Plain, its neritic area, and core sites. (A) General map of the northern SCS and its significant surface circulations. The Chaoshan Plain and its adjacent neritic area are outlined by a solid red line rectangle. The surface circulations in the northern SCS were adapted from Zhang et al. (2022). The SCSBK abbreviation denotes the SCS Branch of Kuroshio, and the black numbers represent major modern surface currents, as follows: 1: Guangdong Coastal Current, 2: SCS Warm Current, 3: Loop Current, and 4: Coastal Current. (B) The major area of the Chaoshan Plain, include the Lianjiang River, Hanjiang River, and Rongjiang River plains. Four cores (SY3-1, SY3-2, SY2-2, and HS02) were obtained from the neritic area of the Lianjiang River plain. Core WYZK-06 was from Song et al. (2012), and core CN-01 was from Tang et al. (2018). Base maps from <http://www.gscloud.cn> and <https://www.ngdc.noaa.gov/mgg/global/global.html>.

thick (Xu et al., 2009; Zheng et al., 2010). The thickness of the Holocene deposits in from the northern South China Sea (SCS) are around 10 m (Wang et al., 2020). The sedimentation characteristics of these regions revealed that aggradation was the dominant process in the eastern continental shelf of China since the Holocene. The Chaoshan Plain is located in southeastern China and borders the northeastern South China Sea (NESCS). The Quaternary deposits in the Chaoshan plain reach a maximum thickness of about 141 m (Chen W., 1984; Song et al., 2012). Several investigations on the Quaternary sediments have been conducted in the Chaoshan plain using multi proxy dating techniques (Chen G., 1984; Li et al., 1987; Li et al., 1988; Zong, 1992; Zheng and Li, 2000; Song et al., 2012; Tang et al., 2018; Zhong et al., 2022). On the contrary, core and chronological data from the adjacent neritic area are limited. The lack of information on sedimentary structures and ages in the area has hindered thorough comprehension of the sedimentary evolution of the Chaoshan region. It remains unclear how many transgressive layers have formed in this area since the Holocene and whether aggradation or incision has been the dominant process since that time. Additionally, the contribution of the sea-level changes and/or tectonic activities on sedimentary process are still debated. The present study employed the optically stimulated luminescence (OSL) dating method to determine the age of the Quaternary sediments from four cores in the neritic area of the Lianjiang River plain, namely, SY2-2, SY3-1, SY3-2, and HS02. The chronological data obtained from these cores will provide an opportunity to understand the timing of the deposition of the Quaternary sediments and factors that led to its formation in the region.

2 Geological setting and sample collection

The SCS is located at the intersection of Eurasia, India-Australia, and the Philippine Sea plates, and is considered as the largest marginal sea in East Asia (Xia et al., 2020). The Chaoshan plain is lying at the NESCS and composed of three major sub-plains, the Lianjiang River plain, the Rongjiang River plain, and the Hanjiang River plain (Figure 1). The Lianjiang River plain extends to about 50 km inland, with a drainage area of up to 838.5 km² and water discharge amounts of approximately 587 million m³/yr (Tang et al., 2018). It characterized by warm-and-wet zone influenced by the East Asian summer monsoon (EASM), with an annual temperature of 22.3°C on average and annual precipitation from 1800 to 2,100 mm (Tang et al., 2018). Differential uplifting–subsidence movement from the Neogene to the early Quaternary has changed the Lianjiang River plain into a faulted basin (Chen W., 1984). Therefore, the Lianjiang River plain has a large accommodation space for the Quaternary deposition, and the thickness of sedimentary sequences reaches up to 141 m (Chen W., 1984; Li et al., 1987; Wang et al., 1997).

Four borehole cores were obtained by rotary drilling from the neritic area of the Lianjiang River plain (Figure 1), i.e., HS02 (116°44'6.51" E, 22°52'10.67" N), SY3-1 (116°43'56.05" E, 22°54'7.07" N), SY3-2 (116°43'57.32" E, 22°54'6.44" N), and SY2-2 (116°46'44.2" E, 22°54'37.36" N). The drilling sites are at an altitude that ranging between 29 and 34 m below mean sea level (bmsl), and core lengths range from 95.15 m to 95.35 m. Details of core lithology are shown in Supplementary Table S1. Seventeen OSL samples were collected from cores SY2-2, SY3-1, SY3-2, and HS02. Despite the



sampling difficulties that prevented high-resolution sampling, this limitation does not affect the scientific discussion presented in our study.

3 OSL dating

3.1 Samples pretreatment

Seventeen OSL samples were treated with 10% HCl and 30% H₂O₂ successively to remove carbonates and organic materials. Wet sieving was utilized to obtain coarse-grained fractions (90–125 μm) according to availability. 90–125 μm fractions were treated with 40% HF for ~40 min to remove feldspar and washed with 10% HCl for about 30 min to remove the fluoride precipitation generated during etching. The purity of quartz fractions was tested by the infrared stimulated luminescence (IRSL) signals.

3.2 D_e determination

90–125 μm quartz fractions were mounted on the center (5 mm diameter) of 9.7-mm diameter stainless-steel discs using silicone oil for equivalent dose (D_e) measurements. Irradiation, preheating, and OSL measurements were conducted on a Risø TL/OSL-DA-20 reader equipped with a ⁹⁰Sr/⁹⁰Y beta source and blue LEDs (λ = 470 ± 20 nm) (Botter-Jensen et al., 1999). All quartz signals were stimulated at 130 °C for 40 s and recorded by an EMI 9235QA

photomultiplier tube fitted with a 7.5-mm Hoya U-340 filter. The D_e in this study was measured by the SAR-SGC method (Lai and Ou, 2013), a combination of single aliquot regenerative dose (SAR) protocol (Murray and Wintle, 2000) and standard growth curve (SGC) method (Roberts and Duller, 2004; Lai, 2006). The preheat for natural and regenerative dose signals was 260 °C for 10 s (Wintle and Murray, 2006), and the preheat for test doses response was 220 °C for 10 s. Preheat plateau test and dose recovery test results from this study and neighboring Pearl River Delta showed that preheat temperature at 260 °C for 10 s was appropriate for dating (Xu et al., 2020; Lin et al., 2022; Xu et al., 2022; Lin et al., 2023). For samples SY3-2-G01, SY3-2-G02, SY3-2-G03, and those from core SY2-2, 6 aliquots were measured using the SAR protocol, and 12 aliquots were measured for the natural L_N/T_N measurement. Given the saturation of the OSL signal in samples from cores SY3-2 and SY2-2, the D_e value of samples SY3-2-G04, SY3-2-G05, and samples from cores SY3-1, HS02 were determined based solely on the natural L_N/T_N measurement to expedite the measurement process. After eliminating any obvious statistical outliers, the final D_e value for a sample was calculated.

3.3 Quartz luminescence characteristics

Tests including the preheat plateau, dose recovery, recycling ratio, and recuperation were conducted on sample SY3-2-G01 to examine the suitability of luminescence properties for the SAR protocol (Wintle and Murray, 2006).

The preheat plateau test was conducted with a preheat temperature ranging from 200 °C to 300 °C with an interval of 20 °C for 10 s and cut-heat temperatures kept at 220 °C for 10 s, using a heating rate of 5 C/s. Twelve aliquots (two aliquots per preheat temperature) were measured at each temperature point. The results indicate a preheat plateau between 260 °C to 280 °C (Figure 2A).

The dose recovery test is to examine whether the D_e measurement protocol can recover a known laboratory dose (Wintle and Murray, 2006). Ideally, the measured dose is in agreement with the given laboratory dose (Wintle and Murray, 2006). The dose recovery test was applied to twelve natural aliquots of sample SY3-2-G01. The given laboratory dose is 20.83 Gy. The measured average D_e value at the 260 °C preheat temperature was 21.3 Gy, resulting in the ratio of dose recovery of 1.02 (Figure 2B). The results are within 10% of the natural dose, indicating that the SAR protocol can recover a laboratory dose.

Recycling ratio and recuperation tests are mainly examining whether no obvious thermal transfer was present and whether sensitivity changes could be well corrected in the measurement (Wintle and Murray, 2006). Research showed that a reliable D_e value can preferably meet two requirements including recuperation < 5% and the recycling ratio within 0.9–1.1 (Wintle and Murray, 2006). The average recycling ratio for sample SY3-2-G01 at the 260 °C preheat temperature was 1.01 (Figure 2C), indicating that the sensitivity changes were well corrected. The recuperation for sample SY3-2-G01 at the 260 °C preheat temperature was 1.7% (Figure 2D), suggesting that no

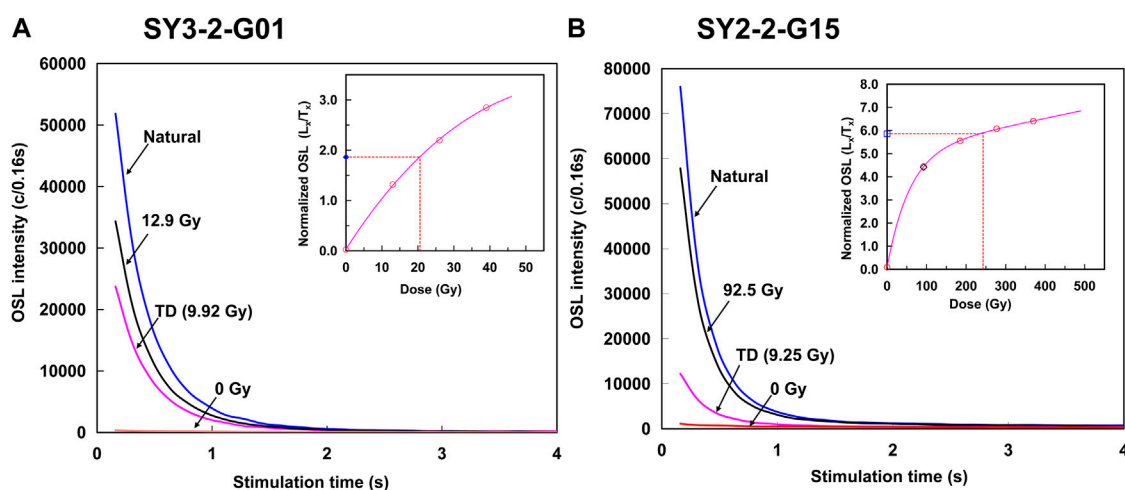


FIGURE 3

OSL decay and growth curves of samples (A) SY3-2-G01 and (B) SY2-2-G15 in the neritic area of the Lianjiang River plain.

obvious thermal transfer was present. Besides, the accepted D_e aliquots for each sample in this study matched the criteria of recycling ratios between 0.9 and 1.1 and recuperation ratios <5%.

3.4 Dose rate measurement

Inductively coupled plasma mass spectrometry (ICP-MS) was used for measuring uranium (U) and thorium (Th). Inductively coupled plasma/optical emission spectrometry (ICP/OES) was utilized for determining potassium (K). The cosmic ray dose was calculated depending on the depth, altitude, and geomagnetic latitude of each sample. The moisture content was estimated to be $25\% \pm 5\%$ for all OSL samples, considering the variation of moisture content within the burial period in the study region. The dose rates and final ages were calculated on the website program DRAC (Durcan et al., 2015).

4 OSL dating results and discussion

4.1 Sediment ages of cores

Representative decay and growth curves of samples SY3-2-G01 and SY2-2-G15 are shown in Figure 3. The decay curves show that OSL intensity decreasing rapidly during the first second of stimulation toward background levels, indicating that the OSL signals are dominated by the fast component in these samples (Wintle and Murray, 2006). The well-fitted growth curves show that the combined SAR-SGC protocol is appropriate for all the samples in this study. Our quartz OSL results from the four cores are listed in Table 1 and can be shown in Figure 4, with ages ranging from 4.9 ± 0.3 ka to 139 ± 28 ka. Quartz OSL signal

saturation could be observed in sixteen samples, with D_e exceeding 190 Gy, indicating that the obtained dating results are regarded as minimum ages (Lai, 2010; Murray et al., 2021; Long et al., 2022; Xu et al., 2022).

The D_e is usually saturates at ~ 150 Gy, resulting in age underestimation for sediments over 50 ka (Buylaert et al., 2007; Lai, 2010; Timar-Gabor et al., 2011; Lai and Fan, 2014; Chapot et al., 2016). Underestimation of quartz OSL age is common in coastal deposits. OSL and thermally transferred OSL (TT-OSL) signals of quartz samples from the coastal plain of Israel demonstrated that the upper limit of quartz D_e from Nilotic origin is close to 140 Gy (Faershtein et al., 2019). In the western Bohai Sea (China), the D_e values of quartz OSL samples are >200 Gy, resulting in ages saturation at >80 ka (Long et al., 2022). Core HPQK01 in the Pearl River Delta also showed that quartz OSL ages ranging from 125 ± 18 ka to 58 ± 6 ka are considered as minimum ages due to the OSL signal saturation >150 Gy (Xu et al., 2022). Age underestimation of fine quartz ($11\text{--}44 \mu\text{m}$) from the Lianjiang River plain occurred on samples older than ~ 130 ka (Tang et al., 2018). Our results suggest that the quartz OSL ages older than ~ 60 ka are underestimated as a result of signal saturation (~ 180 Gy).

4.2 Poor preservation of the late Quaternary sediments

The OSL dating results obtained from core sediments in the neritic area of the Lianjiang River plain suggest that the timing of deposition is between 4.9 ± 0.3 ka and $>83.6 \pm 6.5$ ka, with sedimentation thickness of less than 6.4 m since at least MIS 5 (Figure 4). The sediment thickness in the inner Lianjiang River plain is at least 80 m since MIS 5, which gradually decreases to less than 20 m thick in the outer Lianjiang River plain (Song et al., 2012; Tang et al., 2018) (Figure 5). In the neritic area of the

TABLE 1 OSL dating results from cores SY3-1, SY3-2, SY2-2, and HS02, in the neritic area of the Lianjiang River plain.

Sample ID	Depth (m)	Grain size (μm)	Aliquot number	Moisture (%)	U (ppm)	Th (ppm)	K (%)	Dose rate (Gy/ka)	De (Gy)	Age (ka)
SY3-1-G02	19.1	90–125	3 ^a	25 ± 5	3.2 ± 0.16	14.22 ± 0.71	2.06 ± 0.21	2.98 ± 0.17	321 ± 16	>107.6 ± 8.2
SY3-2-G01	0.6	90–125	4 ^b + 10 ^a	25 ± 5	5.07 ± 0.25	15.57 ± 0.78	2.08 ± 0.21	3.57 ± 0.18	17.6 ± 0.5	4.9 ± 0.3
SY3-2-G02	4.8	90–125	4 ^b + 8 ^a	25 ± 5	2.25 ± 0.11	11.29 ± 0.56	1.97 ± 0.2	2.66 ± 0.15	222 ± 12	>83.6 ± 6.5
SY3-2-G03	6.5	90–125	6 ^b + 6 ^a	25 ± 5	1.79 ± 0.09	9.47 ± 0.47	1.84 ± 0.18	2.36 ± 0.14	229 ± 18	>97.1 ± 9.6
SY3-2-G04	10.2	90–125	5 ^a	25 ± 5	3.9 ± 0.2	16.92 ± 0.85	2.16 ± 0.22	3.37 ± 0.18	239 ± 41	>71 ± 12.7
SY3-2-G05	14.4	90–125	7 ^a	25 ± 5	4.1 ± 0.2	15.75 ± 0.79	2.25 ± 0.22	3.39 ± 0.18	243 ± 33	>71.7 ± 10.4
SY2-2-G15	5.45	90–125	6 ^b + 5 ^a	25 ± 5	2.27 ± 0.11	9.47 ± 0.47	1.75 ± 0.18	2.39 ± 0.14	236 ± 23	>98.9 ± 11.1
SY2-2-G14	14.95	90–125	6 ^b + 7 ^a	25 ± 5	2.97 ± 0.15	13.79 ± 0.69	2.21 ± 0.22	3.05 ± 0.17	227 ± 16	>74.6 ± 6.8
SY2-2-G13	19.55	90–125	6 ^b + 4 ^a	25 ± 5	4.05 ± 0.2	14.72 ± 0.74	2.01 ± 0.2	3.12 ± 0.17	402 ± 69	>129 ± 23
SY2-2-G12	28.45	90–125	6 ^b + 5 ^a	25 ± 5	3.46 ± 0.17	13.18 ± 0.66	2.23 ± 0.22	3.09 ± 0.18	312 ± 30	>101 ± 11.3
SY2-2-G10	43.35	90–125	2 ^b + 5 ^a	25 ± 5	3.78 ± 0.19	10.2 ± 0.51	1.64 ± 0.16	2.52 ± 0.13	334 ± 20	>133 ± 11
SY2-2-G09	47.75	90–125	2 ^b + 4 ^a	25 ± 5	3.81 ± 0.19	18 ± 0.9	2.17 ± 0.22	3.36 ± 0.18	335 ± 26	>99.7 ± 9.4
SY2-2-G07	64.05	90–125	3 ^b + 6 ^a	25 ± 5	3.17 ± 0.16	14.24 ± 0.71	1.96 ± 0.2	2.87 ± 0.16	334 ± 28	>117 ± 12
SY2-2-G03	73.45	63–125	6 ^b + 5 ^a	25 ± 5	3.59 ± 0.18	17.62 ± 0.88	2.59 ± 0.26	3.63 ± 0.21	506 ± 96	>139 ± 28
HS02-G01	6.4	90–125	9 ^a	25 ± 5	2.7 ± 0.14	11.73 ± 0.59	2.06 ± 0.21	2.82 ± 0.16	233 ± 27	>82.6 ± 10.6
HS02-G02	10.5	90–125	4 ^a	25 ± 5	3.18 ± 0.16	14.65 ± 0.73	2.11 ± 0.21	3.07 ± 0.17	197 ± 38	>64.2 ± 13
HS02-G03	12.7	90–125	3 ^a	25 ± 5	2.93 ± 0.15	13.47 ± 0.67	2.21 ± 0.22	3.03 ± 0.17	249 ± 11	>82.1 ± 6

a Numbers of aliquots measured using the standard SGC, method.
 b Numbers of aliquots measured using the standard SAR, method.

Lianjiang River plain, the Holocene sediments are around the same thickness as those in the outer Lianjiang River plain, less than 4.2 m (Tang et al., 2018) (Figure 5). However, core sediments at depths of 12.9 m, 18 m, and 19.4 m were dated to 1,442 ± 65 cal a BP, 11,712 ± 508 cal a BP, and 9,321 ± 221 cal a BP, respectively, indicating that nearly 20 m thick of the Holocene sedimentation formed in the neritic area between the Chaoshan plain and Nanao Island (Sun et al., 2007). The Bohai Sea and the China Sea contain the Holocene sediments that are more than 12 m thick (Liu et al., 2017; Long et al., 2022), while they are thinner in the SCS, around 10 m (Wei et al., 2015; Wang et al., 2020). The neritic area of the Lianjiang River plain has comparatively poor conditions for sedimentary

preservation. The preservation of the late Quaternary sediments in the Lianjiang River plain is still debated. Some studies attributed it to tectonic activities, while others suggested the corresponding of the sea-level variations (Song et al., 2012; Tang et al., 2018).

The South China Block comprises four NE-trending faults, namely, the Littoral, Changle-Nan’ao, Zhenghe-Dabu, and Shaowu-Heyuan-Yangjiang faults (Figure 6) (Sun et al., 2014; Wang et al., 2014). Of these faults, the Littoral and Changle-Nan’ao faults are active since the Quaternary, and have a significant impact on the Lianjiang River plain and its neritic area (Xu et al., 2010; Wang et al., 2014). These faults have influenced sedimentary evolution and paleo-depositional

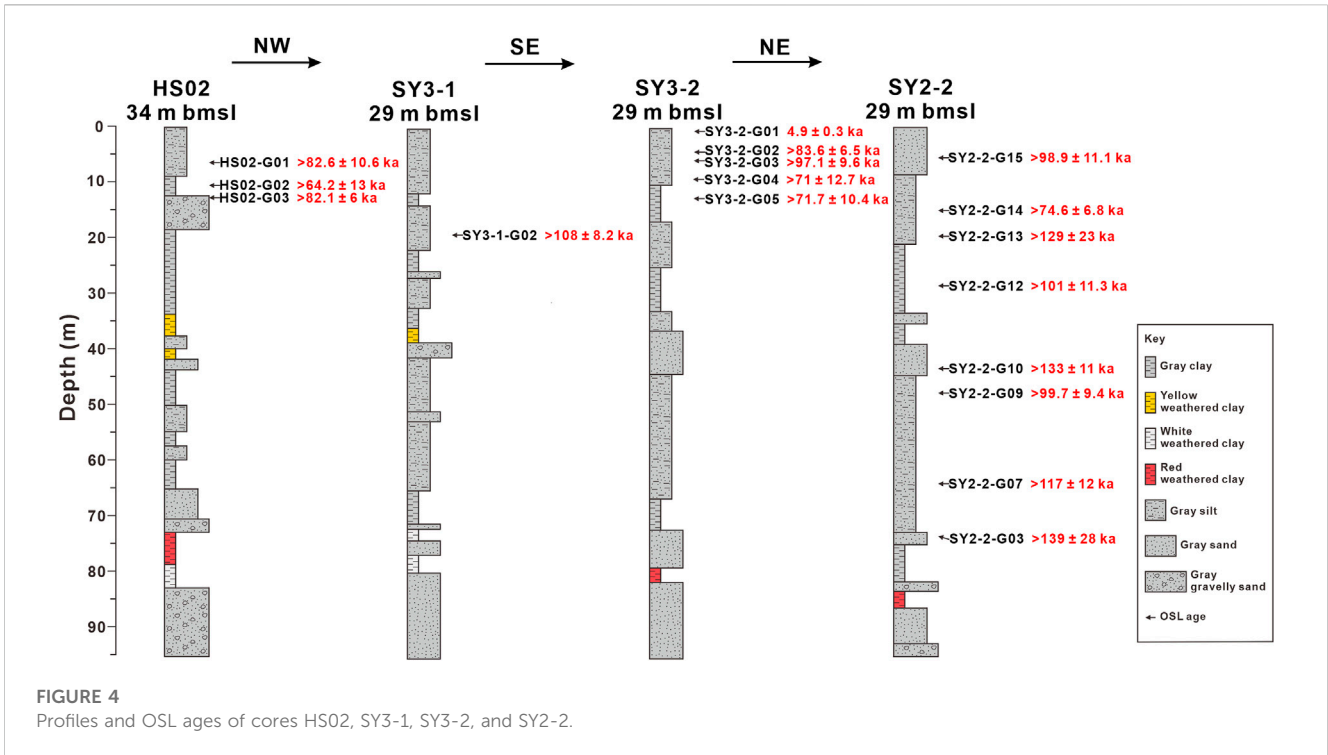


FIGURE 4 Profiles and OSL ages of cores HS02, SY3-1, SY3-2, and SY2-2.

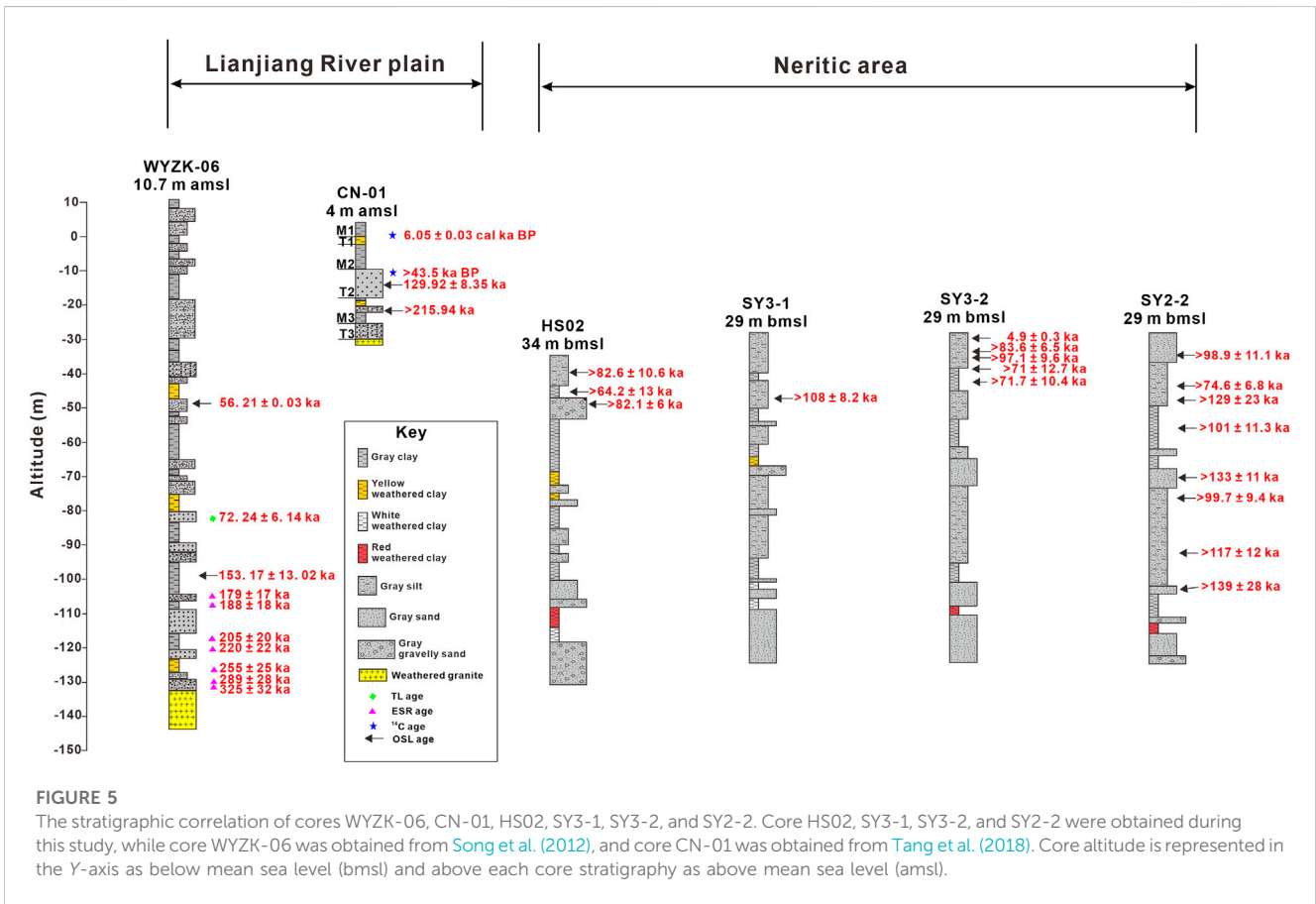
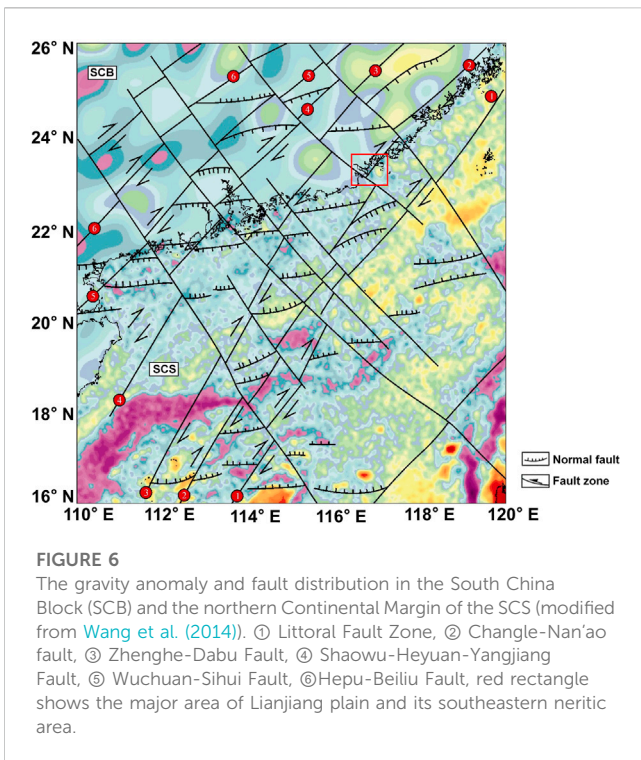


FIGURE 5 The stratigraphic correlation of cores WYZK-06, CN-01, HS02, SY3-1, SY3-2, and SY2-2. Core HS02, SY3-1, SY3-2, and SY2-2 were obtained during this study, while core WYZK-06 was obtained from Song et al. (2012), and core CN-01 was obtained from Tang et al. (2018). Core altitude is represented in the Y-axis as below mean sea level (bmsl) and above each core stratigraphy as above mean sea level (amsl).



environments, resulting in accumulation and transportation of the Quaternary along the faults (Sun et al., 2007).

However, the southeastern neritic area of the Lianjiang River plain is under intense interaction of the SCS and Lianjiang River. Global sea level declined since the end of the last interglacial period and reached the maximum at ca. 130 m bmsl during the last glacial maximum (LGM; ca. 30–20 ka) (Hanebuth et al., 2006; Hodgson et al., 2006; Lambeck et al., 2014; Spratt and Lisiecki, 2016). Low-stand sea level led to the incision of the Lianjiang

River and the exposure of the continental shelf in the northern SCS (Wei et al., 2015; Xu et al., 2019). A series of buried paleochannels extending from the southeastern neritic area of the Lianjiang River plain to approximately 25 km offshore were discovered and considered as the paleo-Lianjiang River (Figure 7) (Liu et al., 2005). The cores in this study are located at the southern part of the paleo-channels of the Lianjiang River, where they likely experienced fluvial incision during the last glacial period. Lan et al. (1991) demonstrated that the medium coarse sands in the Taiwan Shoal were mainly transported by the currents from the coastal region of southeastern China during 10–20 ka BP based on the ¹⁴C dating. Sediments from the core sites were largely transported to the Taiwan Shoal by the Hanjiang diluted water and Guangdong Coastal Currents (Figure 1A), resulting in limited sediments in the neritic area of the Lianjiang River plain (Lan et al., 1991; Lian and Li, 2011). Studies have shown that terrigenous sediments can be transported and spread by oceanic currents once they enter continental margins (Liu et al., 2008; Liu Z. et al., 2016; Zhang et al., 2022). For instance, the sediment from the Pearl River is predominantly transported southwestward via coastal currents, while Taiwan-derived sediments are among the principal contributors in the NESCS due to the influence of deep-water currents and surface currents that vary seasonally (Liu Z. et al., 2016; Zhang et al., 2022). Therefore, fluvial incision during the last glacial period and strong transportation by coastal currents may result in poor preservation of sediments since at least 83.6 ka in the study area.

The Chaoshan plain neritic area experienced poor sediment preservation since MIS 5, while other regions experienced transgressions and regressions resulting in more than 30 m thick of deposition. Studies from the Bohai Sea, the western South Yellow Sea, and the East China Sea have revealed evidence of sea-level changes and their impact on sedimentary processes (Liu J. et al., 2016; Liu et al., 2017; Wang et al., 2019; Wang et al., 2020; Long et al.,

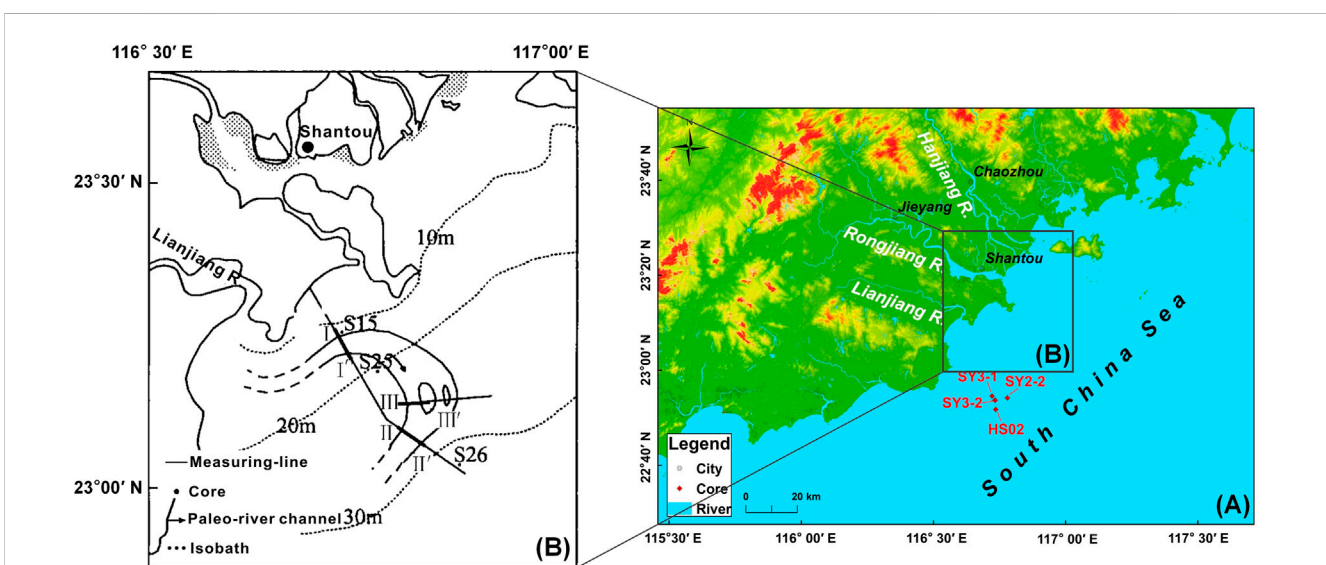


FIGURE 7
(A) The major area of Lianjiang River plain and its southeastern neritic area in this study. (B) Location of the paleo-river channel of paleo Lianjiang River in the neritic area of the modern Lianjiang River mouth, modified from Liu et al. (2005).

2022). Further research indicated that sea-level changes were identified as the primary control for sedimentation on the northeastern SCS, with Kuroshio intrusion being responsible for the transport of Taiwan-derived sediment during the late Quaternary (Zhang et al., 2022). In summary, the sedimentary processes in the eastern continental shelf of China were mainly influenced by sea-level changes.

5 Conclusion

In this study, we used quartz OSL technique to date the Quaternary sediments from cores SY2-2, SY3-1, SY3-2, and HS02 in the neritic area of the Lianjiang River plain. Seventeen dates ranged from 4.9 ± 0.3 ka to $>139 \pm 28$ ka. Except for SY3-2-G01, all samples were considered minimum ages due to De saturation (>190 Gy). Our findings reveal that the sediments have been poorly preserved for at least 83.6 ka, with a sedimentation thickness since at least MIS 5 of less than 6.4 m and Holocene sediments of less than 4.2 m. This study has shown that erosion has occurred in the neritic area of the Lianjiang River plain in the NESCS since at least MIS 5 due to fluvial incision caused by low sea levels during the last glacial period and strong coastal currents.

Data availability statement

The original contributions presented in the study are included in the article/Supplementary Material, further inquiries can be directed to the corresponding authors.

Author contributions

JZ: data curation, visualization, writing-original draft. BL: data curation, investigation. YO: data curation, investigation. RT: data curation. JS: data curation, investigation. YX: writing-reviewing and editing. FW: data curation, investigation. MA: reviewing and editing. KZ: investigation. ZL: conceptualization, methodology,

supervision, funding acquisition, reviewing, and editing. All authors contributed to the article and approved the submitted version.

Funding

This research was supported by the Natural Science Foundation of Guangdong Province (2023A1515012926), the National Natural Science Foundation of China (Grants No. 41877438), the STU Scientific Research Start-Up Foundation for Talents (NTF19003, NTF20006), and Innovation and Entrepreneurship Project of Shantou (2021112176541391).

Acknowledgments

We thank Qinjing Shen and Xiaolin Xu for the helpful discussions.

Conflict of interest

The authors declare that the research was conducted in the absence of any commercial or financial relationships that could be construed as a potential conflict of interest.

Publisher's note

All claims expressed in this article are solely those of the authors and do not necessarily represent those of their affiliated organizations, or those of the publisher, the editors and the reviewers. Any product that may be evaluated in this article, or claim that may be made by its manufacturer, is not guaranteed or endorsed by the publisher.

Supplementary material

The Supplementary Material for this article can be found online at: <https://www.frontiersin.org/articles/10.3389/feart.2023.1089946/full#supplementary-material>

References

- Bøtter-Jensen, L., Duller, G. A. T., Murray, A. S., and Banerjee, D. (1999). Blue light emitting diodes for optical stimulation of quartz in retrospective dosimetry and dating. *Radiat. Prot. Dosim.* 84, 335–340. doi:10.1093/oxfordjournals.rpd.a032750
- Buylaert, J. P., Vandenberghe, D., Murray, A. S., Huot, S., De Corte, F., and Van den Haute, P. (2007). Luminescence dating of old (>70 ka) Chinese loess: A comparison of single-aliquot OSL and IRSL techniques. *Quat. Geochronol.* 2 (1), 9–14. doi:10.1016/j.quageo.2006.05.028
- Chapot, M. S., Roberts, H. M., Duller, G. A. T., and Lai, Z. P. (2016). Natural and laboratory TT-OSL dose response curves: Testing the lifetime of the TT-OSL signal in nature. *Radiat. Meas.* 85, 41–50. doi:10.1016/j.radmeas.2015.11.008
- Chen, G. (1984). Quaternary fault block movement in Chao-Shan Plain. *South China J. Seismol.* 4 (4), 001–018. (in Chinese). doi:10.13512/j.hndz.1984.04.001
- Chen, W. (1984). Several features for the development of sedimentary basin in Chaoshan area, Guangdong province. *South China J. Seismol.* 4 (2), 20–30. (in Chinese). doi:10.13512/j.hndz.1984.02.004
- Chen, X., Li, R., Lan, X., and Xu, X. (2020). Late quaternary stratigraphic sequence and depositional response in the Western Bohai Sea. *Earth Sci.* 45 (7), 2684–2696. (in Chinese with English abstract). doi:10.3799/dqkx.2020.014
- Durcan, J. A., King, G. E., and Duller, G. A. (2015). Drac: Dose rate and age calculator for trapped charge dating. *Quat. Geochronol.* 28, 54–61. doi:10.1016/j.quageo.2015.03.012
- Faershtein, G., Porat, N., and Matmon, A. (2019). Natural saturation of OSL and TT-OSL signals of quartz grains from Nilotic origin. *Quat. Geochronol.* 49, 146–152. doi:10.1016/j.quageo.2018.04.002
- Hanebuth, T. J. J., Saito, Y., Tanabe, S., Vu, Q. L., and Ngo, Q. T. (2006). Sea levels during late marine isotope stage 3 (or older?) reported from the Red River delta (northern Vietnam) and adjacent regions. *Quat. Int.* 145–146, 119–134. doi:10.1016/j.quaint.2005.07.008
- Hodgson, D. A., Verleyen, E., Squier, A. H., Sabbe, K., Keely, B. J., Saunders, K. M., et al. (2006). Interglacial environments of coastal east Antarctica: Comparison of MIS 1 (Holocene) and MIS 5e (last interglacial) lake-sediment records. *Quat. Sci. Rev.* 25 (1–2), 179–197. doi:10.1016/j.quascirev.2005.03.004
- Lai, Z. (2010). Chronology and the upper dating limit for loess samples from Luochuan section in the Chinese Loess Plateau using quartz OSL SAR protocol. *J. Asian Earth Sci.* 37 (2), 176–185. doi:10.1016/j.jseas.2009.08.003

- Lai, Z., and Fan, A. (2014). Examining quartz OSL age underestimation for loess samples from Luochuan in the Chinese Loess Plateau. *Geochronometria* 41 (1), 57–64. doi:10.2478/s13386-013-0138-1
- Lai, Z., and Ou, X. (2013). Basic procedures of optically stimulated luminescence (OSL) dating. *Prog. Geogr.* 32 (5), 683–693. (in Chinese with English abstract). CNKI:SUN:DLKJ.0.2013-05-003.
- Lai, Z. (2006). Testing the use of an OSL standardised growth curve (SGC) for determination on quartz from the Chinese Loess Plateau. *Radiat. Meas.* 41 (1), 9–16. doi:10.1016/j.radmeas.2005.06.031
- Lambeck, K., Rouby, H., Purcell, A., Sun, Y., and Sambridge, M. (2014). sea level and global ice volumes from the last glacial maximum to the Holocene. *Proc. Natl. Acad. Sci. U. S. A.* 111 (43), 15296–15303. doi:10.1073/pnas.1411762111
- Lan, D., Zhang, W., Chen, C., and Xie, Z. (1991). Preliminary study on age and origin of medium-coarse sands in Taiwan Shoal. *Taiwan Strait* 10 (2), 156–161. (in Chinese with English abstract). CNKI:SUN:TWHX.0.1991-02-009.
- Lan, X. H., Ri-Hui, L. I., Chen, X. H., Qin, Y. C., Wang, Z. B., and Bei-Bei, M. I. (2018). Study of sedimentary geochemistry in the western Bohai Sea since late pleistocene. *Adv. Mar. Sci.* 1, 67–78. (in Chinese with English abstract).
- Li, G., Li, P., Liu, Y., Qiao, L., Ma, Y., Xu, J., et al. (2014). Sedimentary system response to the global sea level change in the East China Seas since the last glacial maximum. *Earth-Science Rev.* 139, 390–405. doi:10.1016/j.earscirev.2014.09.007
- Li, P., Huang, Z., Zong, Y., and Zhang, Z. (1987). *Hanjiang Delta*. Beijing: Ocean Press. (in Chinese).
- Li, P. R., Huang, Z. G., and Zong, Y. Q. (1988). New views on geomorphological development of the Hanjiang River Delta. *Acta Geogr. Sin.* 55 (1), 19–34. (in Chinese). doi:10.11821/xb198801003
- Lian, Y. K., and Li, Y. (2011). Grain size characteristics and transport trend in the Taiwan Bank. *J. Oceanogr. Taiwan Strait* 30 (1), 122–127. (in Chinese with English abstract). doi:10.3969/j.issn.1000-8160.2011.01.018
- Lin, P., Song, Y., Zhan, W., Tian, R., Wang, Z., Xu, X., et al. (2023). Late Pleistocene to Holocene sedimentary history in the Pearl River Delta revealed by OSL and radiocarbon dating. *Catena* 224, 106972. doi:10.1016/j.catena.2023.106972
- Lin, P., Xu, X., Yan, C., Luo, L., and Lai, Z. (2022). Holocene sedimentary of the Pearl River Delta in South China: OSL and radiocarbon dating of cores from zhuhai. *Front. Mar. Sci.* 2260. doi:10.3389/fmars.2022.1031456
- Liu, A., Lü, W., and Cai, F. (2005). A buried meandering river of late quaternary off Shantou city, Guangdong province. *Oceanol. Limnologia Sinica* 36 (2), 104–110. (in Chinese with English abstract). CNKI:SUN:HYFZ.0.2005-02-001.
- Liu, J., Saito, Y., Kong, X., Wang, H., Wen, C., Yang, Z., et al. (2010). Delta development and channel incision during marine isotope stages 3 and 2 in the Western South Yellow Sea. *Mar. Geol.* 278 (1), 54–76. doi:10.1016/j.margeo.2010.09.003
- Liu, J., Wang, H., Wang, F., Qiu, J., Saito, Y., Lu, J., et al. (2016). Sedimentary evolution during the last ~1.9Ma near the Western margin of the modern Bohai Sea. *Palaeogeogr. Palaeoclimatol. Palaeoecol.* 451, 84–96. doi:10.1016/j.palaeo.2016.03.012
- Liu, S., Mi, B., Fang, X., Li, X., Pan, H.-J., Chen, M.-T., et al. (2017). A preliminary study of a sediment core drilled from the mud area on the inner shelf of the East China Sea: Implications for paleoclimatic changes during the fast transgression period (13 ka B.P.–8 ka B.P.). *Quat. Int.* 441, 35–50. doi:10.1016/j.quaint.2016.09.057
- Liu, Z., Tuo, S., Colin, C., Liu, J. T., Huang, C.-Y., Selvaraj, K., et al. (2008). Detrital fine-grained sediment contribution from Taiwan to the northern South China Sea and its relation to regional ocean circulation. *Mar. Geol.* 255 (3), 149–155. doi:10.1016/j.margeo.2008.08.003
- Liu, Z., Zhao, Y., Colin, C., Stattegger, K., Wiesner, M. G., Huh, C.-a., et al. (2016b). Source-to-sink transport processes of fluvial sediments in the South China Sea. *Earth-Science Rev.* 153, 238–273. doi:10.1016/j.earscirev.2015.08.005
- Long, Z., Wang, Z., Tu, H., Li, R., Wen, Z., Wang, Y., et al. (2022). OSL and radiocarbon dating of a core from the Bohai Sea in China and implication for Late Quaternary transgression pattern. *Quat. Geochronol.* 70, 101308. doi:10.1016/j.quageo.2022.101308
- Murray, A., Arnold, L. J., Buylaert, J.-P., Guérin, G., Qin, J., Singhvi, A. K., et al. (2021). Optically stimulated luminescence dating using quartz. *Nat. Rev. Methods Prim.* 1 (1), 72. doi:10.1038/s43586-021-00068-5
- Murray, A. S., and Wintle, A. G. (2000). Luminescence dating of quartz using an improved single-aliquot regenerative-dose protocol. *Radiat. Meas.* 32 (1), 57–73. doi:10.1016/S1350-4487(99)00253-X
- Qin, Y.-C., Wang, Z., Jiang, X., Zhang, X., and Luan, X. (2023). Quantitative sediment provenance of the northwestern East China Sea: Evidence for tidal current-driven offshore transport and paleogeographic implications. *Geomorphology*, 108668. doi:10.1016/j.geomorph.2023.108666
- Roberts, H., and Duller, G. A. (2004). Standardised growth curves for optical dating of sediment using multiple-grain aliquots. *Radiat. Meas.* 38 (2), 241–252. doi:10.1016/j.radmeas.2003.10.001
- Song, Y., Chen, W., Pan, H., Zhang, Z., He, Z., Chen, X., et al. (2012). Geological age of Quaternary series in Lianjiang plain. *J. Jilin Univ.(Earth Sci. Ed.)* 42, 154–161. (in Chinese with English abstract). doi:10.13278/j.cnki.jjuese.2012.s1.040
- Spratt, R. M., and Lisiecki, L. E. (2016). A Late Pleistocene sea level stack. *Clim. Past* 12 (4), 1079–1092. doi:10.5194/cp-12-1079-2016
- Sun, J.-I., Xu, H.-I., Wu, P., Wu, Y.-b., Qiu, X.-l., and Zhan, W.-h. (2007). Late Quaternary sedimentological characteristics and sedimentary environment evolution in sea area between Nan'ao and Chenghai, eastern Guangdong. *J. Trop. Oceanogr.* 26, 30–36. (in Chinese with English abstract). doi:10.3969/j.issn.1009-5470.2007.03.005
- Sun, X. M., Zhang, X. Q., Zhang, G. C., Lu, B. L., Yue, J. P., and Zhang, B. (2014). Texture and tectonic attribute of Cenozoic basin basement in the northern South China Sea. *Sci. China Earth Sci.* 57 (6), 1199–1211. doi:10.1007/s11430-014-4835-2
- Tang, Y., Zheng, Z., Chen, C., Wang, M., and Chen, B. (2018). Evolution of the Lian River coastal basin in response to Quaternary marine transgressions in Southeast China. *Sediment. Geol.* 366, 1–13. doi:10.1016/j.sedgeo.2018.01.003
- Timar-Gabor, A., Vandenberghe, D. A. G., Vasiliniuc, S., Panaoitu, C. E., Panaiotu, C. G., Dimofte, D., et al. (2011). Optical dating of Romanian loess: A comparison between silt-sized and sand-sized quartz. *Quat. Int.* 240 (1), 62–70. doi:10.1016/j.quaint.2010.10.007
- Wang, F., Wang, F., Zhang, W., Xu, S., and Lai, Z. (2023). A novel machine learning fingerprinting method using sparse representation for provenance detection in delta sediments. *Catena* 227, 107095. doi:10.1016/j.catena.2023.107095
- Wang, J. H., Zheng, Z., and Wu, C. Y. (1997). Sedimentary facies and paleoenvironmental evolution of the late quaternary in the Chaoshan Plain, east Guangdong. *Acta Scifntiarum Nat. Univ. Sunyatseni* 36 (1), 95–100. (in Chinese with English abstract). CNKI:SUN:ZSDZ.0.1997-01-019.
- Wang, L., Li, G., Xu, J., Liu, Y., Qiao, L., Ding, D., et al. (2019). Strata sequence and paleochannel response to tectonic, sea-level, and Asian monsoon variability since the late Pleistocene in the South Yellow Sea. *Quat. Res.* 92 (2), 450–468. doi:10.1017/qua.2019.29
- Wang, X. F., Yu, S., Gong, Y. H., Li, S. Z., Liu, X., Ma, Y., et al. (2014). Extension of NE-trending faults in South China to northern South China sea continental shelf. *Geotect. Metallogenia* 38 (3), 557–570. (in Chinese with English abstract).
- Wang, Z., Zhang, J., Mei, X., Chen, X., Zhao, L., Zhang, Y., et al. (2020). The stratigraphy and depositional environments of China's sea shelves since MIS5 (74-128) ka. *Geol. China* 47 (5), 1370–1394. (in Chinese with English abstract).
- Wei, C., Zhang, K., Yu, Z., and Qiu, Y. (2015). Correlation of stratigraphic sequences between the Pearl River Delta and its offshore continental shelf since the late pleistocene. *Acta Sedimentol. Sin.* 33 (4), 714–723. (in Chinese with English abstract).
- Wintle, A. G., and Murray, A. S. (2006). A review of quartz optically stimulated luminescence characteristics and their relevance in single-aliquot regeneration dating protocols. *Radiat. Meas.* 41 (4), 369–391. doi:10.1016/j.radmeas.2005.11.001
- Xia, S., Zhou, P., Zhao, D., and Cao, J. (2020). Seismogenic structure in the source zone of the 1918 M7.5 NanAo earthquake in the northern South China Sea. *Phys. Earth Planet. Interiors* 302, 106472. doi:10.1016/j.pepi.2020.106472
- Xu, F., Li, A., Xiao, S., Wan, S., Liu, J., and Zhang, Y. C. (2009). Paleoenvironmental evolution in the inner shelf of the East China Sea since the last deglaciation. *Acta Sedimentol. Sin.* 27, 118–127. (in Chinese with English abstract).
- Xu, H. L., Ye, C. M., Qiu, X. L., Sun, J. L., and Xia, S. H. (2010). Studies on the binhai Fault Zone in the northern South China sea by the deep geophysical exploration and its seismogenic structure. *South China J. Seismol.* 30, 10–18. (in Chinese with English abstract).
- Xu, X., Li, H., Tang, L., Lai, Z., Xu, G., Zhang, X., et al. (2020). Chronology of a Holocene core from the Pearl River delta in southern China. *Front. Earth Sci.* 8, 262. doi:10.3389/feart.2020.00262
- Xu, X., Zhong, J., Huang, X., Li, H., Ding, Z., and Lai, Z. (2022). Age comparison by luminescence using quartz and feldspar on core HPQK01 from the Pearl River Delta in China. *Quat. Geochronol.* 71, 101320. doi:10.1016/j.quageo.2022.101320
- Xu, Y. T., Lai, Z. P., and Li, C. A. (2019). Sea-level change as the driver for lake formation in the Yangtze Plain - a review. *Glob. Planet. Change* 181, 102980. doi:10.1016/j.gloplacha.2019.102980
- Zhang, C., Yang, S., Huang, X., Dou, Y., Li, F., Xu, X., et al. (2022). Sea level change and Kuroshio intrusion dominated Taiwan sediment source-to-sink processes in the northeastern South China Sea over the past 244 kyrs. *Quat. Sci. Rev.* 287, 107558. doi:10.1016/j.quascirev.2022.107558
- Zheng, Y., Zheng, H., and Wang, K. (2010). History of sea level change since last glacial: Reflected by sedimentology of core from East China Sea inner shelf. *J. Tongji Univ.* 38 (9), 1381–1386. (in Chinese with English abstract).
- Zheng, Z., and Li, Q. (2000). Vegetation, climate, and sea level in the past 55,000 years, Hanjiang Delta, Southeastern China. *Quat. Res.* 53 (3), 330–340. doi:10.1006/qres.1999.2126
- Zhong, J., Ling, K., Yang, M., Shen, Q., Abbas, M., and Lai, Z. (2022). Radiocarbon and OSL dating on cores from the Chaoshan delta in the coastal South China Sea. *Front. Mar. Sci.* 9. doi:10.3389/fmars.2022.1030841
- Zong, Y. Q. (1992). Postglacial stratigraphy and sea-level changes in the han River Delta, China. *J. Coast. Res.* 8 (1), 1–28. Available at: <https://www.jstor.org/stable/4297948>.